Original Article

Trends in Hearing
2014, Vol. 18: 1–10

DOI: 10.1177/2331216514529189
trh.sagepub.com

Spatial Design of Hearing Aids Incorporating Multiple Vents

Daniel Stevenson[1], Grant Searchfield[2], and Xun Xu[1]

Abstract

The main aim of this study was to investigate the shape variation in the human ear canal and the effects of venting on the spatial design of hearing aids. The second aim was to determine the design feasibility of a multiple venting hearing aid and assess the flexibility of design provided. A statistical shape model based on principal component analysis was created from a dataset of 60 left and 49 right ears. The modal variations of these models were then examined to determine the narrowest portion of the ear canal likely to limit effective venting. Finally, 3D models of two hearing aid shells, one with multiple 0.4-mm vents and the other with a single large 3-mm vent were created. Results showed that more than 50% of the shape variation in the human ear canal can be described by the first three modes of the statistical shape model developed. The narrowest predicted variation of this model had a minimum area of 36.4 mm^2, and the mean ear shape was found to have a minimum area of approximately 48 mm^2. It is estimated that even with a conservative vent packing of 0.4, multiple venting equivalent to at least a single 2-mm vent is achievable. The predicted variation in the human ear canal provides adequate physical space for a feasible multiple vented hearing aid shell. Furthermore, as multiple small vents are able to fit in around other components in the hearing aid design, certain design flexibility is provided by this venting approach.

Keywords

hearing aid, design, multiple vents

Introduction

Venting is incorporated into hearing aid design to perform pressure equalization and reduce occlusion effects. Traditional venting of a single parallel vent channel, running from the base plate to the end plate of the hearing aid, is still widely used in hearing aid fitting. Vent diameters vary but normally range between 1 and 3 mm. A number of studies have been conducted looking at the acoustics of various hearing aid venting styles including traditional parallel vents, reverse horn vents, Y vents, and open fitting hearing aids (Kiessling, Brenner, Jespersen, Groth, & Jensen, 2005; Kuk, Keenan, & Lau, 2005, 2009; Kuk, Keenan, Lau, Dinulescu, et al., 2005; Stuart, Allen, Downs, & Carpenter, 1999; Studebaker & Cox, 1977). Most studies focus on the acoustic properties of these vents with little comment about the spatial interactions within the hearing aid or earmold. However, some vents such as diagonal or Y vents and external trench vents have been recommended as particularly useful for those with narrow ear canals (Dillon, 2001; Studebaker & Cox, 1977; Valente, Hosford-Dunn, & Roeser, 2008). Diagonal vents branch diagonally off the sound bore in hearing aid earmolds rather than running parallel to it. This has been shown to limit the high frequency gain available to the hearing aid (Studebaker & Cox, 1977). As such, diagonal vents have been recommended to be used only in cases where there is not enough space for other venting styles.

The authors have proposed an alternative venting configuration that uses multiple small vents as opposed to a single large vent. An earlier publication by the authors looking at the acoustics of multiple vented earmolds concluded that multiple vented earmolds are capable of achieving similar feedback and occlusion performance but are likely to require a greater area to achieve this venting (Stevenson, Searchfield, Dodd, & Xu, 2013).

[1]Department of Mechanical Engineering, University of Auckland, New Zealand
[2]Audiology Section, University of Auckland, New Zealand

Corresponding author:
Grant Searchfield, Audiology Section, University of Auckland, Private Bag 92019, Auckland 1142, New Zealand.
Email: g.searchfield@auckland.ac.nz

This article explores the spatial constraints of a universal in-the-ear hearing aid and the feasibility of a multiple vented configuration within the predicted ear canal shape variations. Understanding of shape and spatial requirements is critical in the design of hearing aids that are comfortable as well as providing good retention and acoustic seal with the ear canal. To take advantage of a specific venting configuration, non-reproducible slit leakages around the ear must be reduced. Unlike customized hearing aids, when designing for a universal style device or a one-size-fits-many device, exact representation of each ear canal cannot be used. As such, one must obtain an understanding of the variances within the target population and design for these variances.

Shape Data Modeling and Analysis

Statistical Shape Model

A statistical shape model has been used to define the shape variations of the ear canal within the population. The statistical shape model used is based on Cootes, Edwards, and Taylor (1998, 2001), Hutton, Buxton, and Hammond (2001), and Paulsen, Larsen, Nielsen, Laugesen, and Ersbøll (2002). Principal component analysis (PCA) of a set of thin plate spline-wrapped ear impression scans was used to determine the main modes of variation within the dataset.

A set of 60 left ears and 49 right ears has been used in the model to assess expected shape variation within the ear canal. On each of the scans in the dataset, 15 landmark points were identified. Figure 1 shows a sample landmarked shape. Numbers mark the superior, inferior, anterior, and posterior points on the first (1–4) and second bends (5–8) identified as the points of maximum curvature of the ear canal. Landmark point 9 is located at the crus of the helix where the antihelix meets the helix. Point 10 relates to the point where the helix meets the plane of the concha, and point 11 is the point directly opposite this on the edge of the concha. Finally, points 12–15 are evenly placed along the edge of the concha defined as the area of maximum curvature along the antihelical path.

A template mesh is then wrapped to each shape instance using the landmarked points through a thin plate spline technique. Wrapped data are then aligned in 3D space using Procrustes alignment, and PCA is performed. PCA gives the eigenvectors describing the modes of variation and the eigenvalues describing the relative importance of each mode. For a review of PCA, Procrustes alignment, and thin plate spline techniques, see Bookstein (1989), Cootes, Taylor, Cooper, and Graham (1995), Hutton et al. (2001), Jolliffe (1986), Lorenz and Krahnstöver (2000).

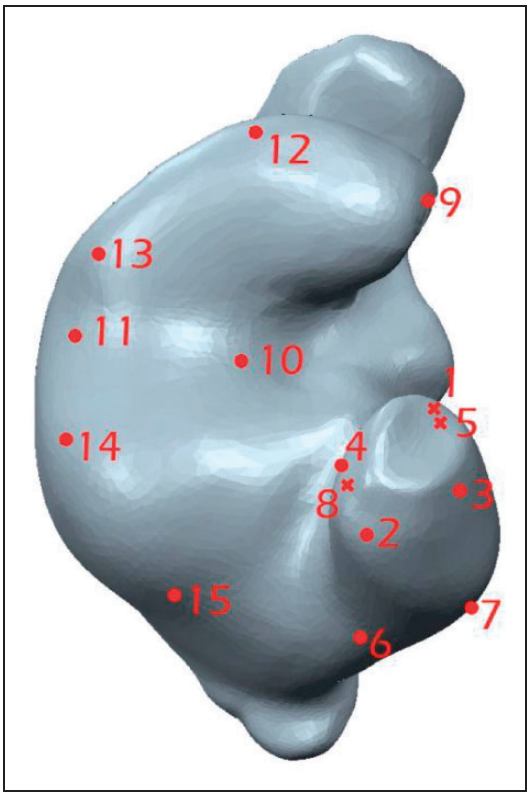

Figure 1. Mesh showing 15 landmark locations on sample ear-mold scan, Xs representing landmark points hidden from view.

Minimum Cross-sectional Area

Given that a hearing aid pressure equalizing vent is required to provide a path for sound from one side of a hearing aid to the other, the spatially limiting factor is likely to occur at the narrowest point in the ear canal. We will call this point the minimum cross-sectional area. To determine the minimum cross-sectional area, a series of cross sections were taken normal to a central axis of the ear canal. The ear canal central axis has been defined by determining the shortest path along the medial sheet between a central point at the top of the ear canal and at the entrance of the ear canal.

The medial sheet forms a part of the medial axis transform. The medial axis transform is a commonly used 3D shape descriptor for shape recognition, modeling, and manipulation (Crimi et al., 2011; Gerig, Styner, Shenton, & Lieberman, 2001; Styner & Gerig, 2001a, 2001b). Shapes are represented by a set of maximal medial balls within the interior of the solid (M-rep) as opposed to the points on the boundary (B-rep; Crimi et al., 2011; Pizer, Thall, & Chen, 1999; Styner & Gerig, 2001b). Maximal medial balls are the largest sphere that does not contain points on the surface of the shape and are not contained completely within another medial ball. The center of the medial ball is a

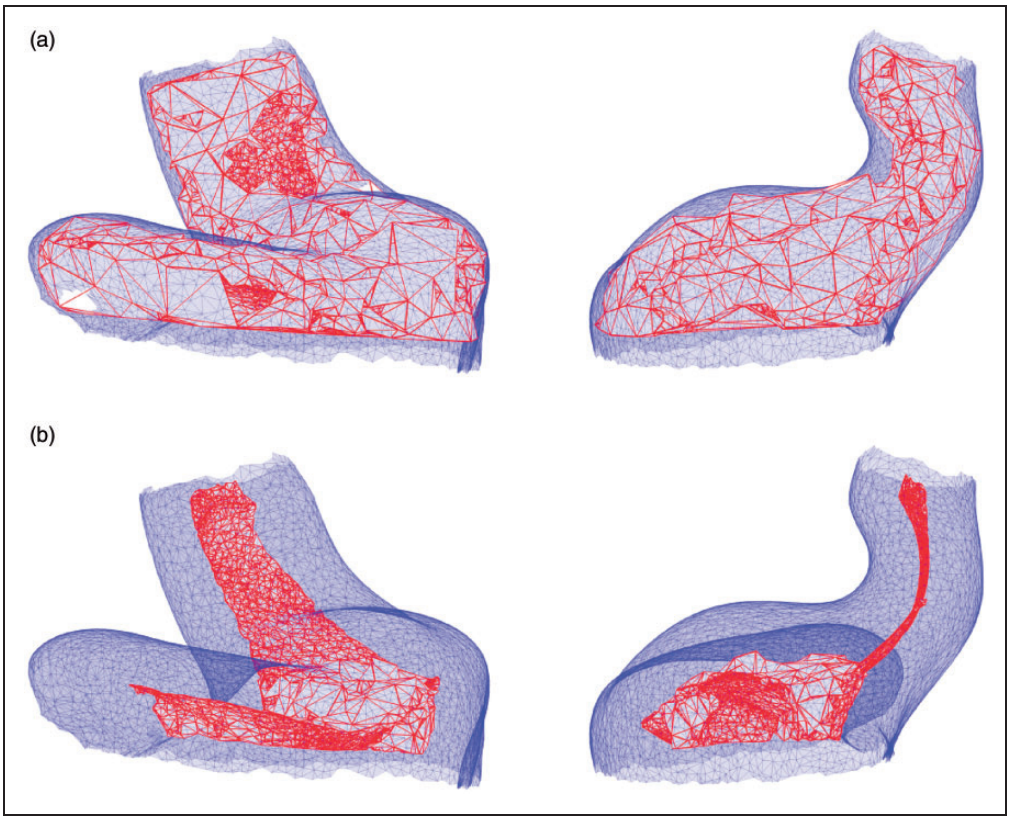

Figure 2. Plots showing medial sheet for the mean left ear generated from medial balls with radius *r* greater than or equal to (a) 0 mm and (b) 3 mm.

point that has two or more closest points on the surface. The medial sheet is the union of the center of these medial balls within the shape forming a skeletal sheet structure within the shape.

An approximation of the medial sheet has been obtained through the use of a 3D Voronoi diagram or Voronoi skeleton (Fabbri, Estrozi, & Costa, 2002; Ogniewicz & Ilg, 1992; Styner & Gerig, 2001b). The Voronoi diagram divides the shape into a set of cells with the edges of each cell containing the points equidistant between two shape vertices. The vertices of these Voronoi cells contained within the shape represent the center of the medial balls of the shape. However, Voronoi vertices are also often formed near the surface of the shape far from the medial axis or medial sheet even for very smooth scans. As such, the vertices must be pruned to include only those near the medial axis or center of the shape.

Pruning removes sheet branches of medial skeletons not indicative of the skeleton structure of the shape whilst maintaining the topology of the original shape. A number of different skeleton pruning or thinning algorithms exist for reducing the complexity of medial axis shape representations based on medial or object angle (Dey & Zhao, 2003; Miklos, Giesen, & Pauly, 2010), segmentation by shape significance (Beristain, Graña, & Gonzalez, 2012; Tam & Heidrich, 2003), and the so-called λ-*medial axis method* (Chaussard, Couprie, & Talbot, 2009, 2011; Chazal & Lieutier, 2005). The method selected is similar to that of λ-medial axis that prunes medial balls based on the size of the circumradius of the medial boundary values or closest surface points. In this study, the medial balls were pruned based purely on the radius of the medial balls in question, which is the distance of the medial ball from the surface. Medial balls with radius (*r*) less than or equal to approximately 2 or 3 mm were pruned removing small medial balls describing detailed surface information.

Pruning small medial balls related to surface detail provides a good approximation of the medial axis. For all shapes analyzed, the medial sheet was viewed to assess whether an appropriate *r* was used and that the pruned medial sheet provided a good approximation of the true medial axis. Figure 2 shows the medial sheets generated using *r* of (a) 0 and (b) 3 mm for mean left ear shape. As *r* increased, more of the vertices closer to the surface are removed, and the triangulation on the medial sheet improves, particularly for the ear canal, which is the area of interest. These small radius vertices describe the fine surface detail of the shape not needed in the

medial axis. The method reduced the medial sheet within the ear scan to a thin sheet within the center of the ear canal in the area of interest in the scan (Figure 2b).

A fast marching algorithm that uses a finite difference approximation was used to determine the shortest path along the medial sheet between the two central points. Planar cross sections were taken approximately normal to the ear canal at both the entrance to the ear canal and just beyond the second bend. The centers of gravity of these sections were then taken, and the closest points to these on the medial sheet were used to determine the two end points of the centerline ear canal axis. The fast marching algorithm was then used to determine the shortest path between these two end points along the medial sheet.

The fast marching algorithm has been used for a number of other medical applications involving tubular structures such as vessels, veins, and airways (Antiga, Ene-Iordache, & Remuzzi, 2003; Cárdenes, Bogunovic, & Frangi, 2010; Rouchdy & Cohen, 2011). As the fast marching algorithm allows for calculation of the shortest paths across faces and not just along edges, it was found to provide a smoother centerline and to lead to less variability in curve normals compared with other shortest path methods such as the Dijkstra algorithm. For example, Figure 3 shows the fast marching shortest path on the left mean ear medial sheet.

The Creo 3D solid modeling package (PTC Creo, Needham, MA, USA) was used to create a spline defining the path of fast marching shortest path, and a series of cross sections of the ear canal were taken normal to the spline curve. Eleven evenly spaced cross sections were taken from the bottom of the centerline to the top with distance between the cross sections ranging from 0.88 to 1.78 mm along the centerline curve. From these, a cross-sectional area profile of each studied shape was determined. The cross section approximating the point of the second and first bends was identified and the relative centerline distance between these two features determined.

A closed cross-sectional area could not always be achieved. The plane normal to the centerline curve would sometimes section the scan mesh outside of the ear canal into the concha and outside the ear itself. This occurred more in wider canal shapes that had a sharp first bend of the ear canal.

Results

Shape Model

The modes of variation of the left and right data models against the percentage of variation in the training dataset explained by each mode are shown in Figure 4. The first mode explains 23% of the variation in the left ear shapes and 32% of variation in the right ears. More than 50% of the variation in both datasets is explained by the first three modes of variation. This shows similar results to that observed by Paulsen et al. (2002), who used scans of 29 ear impressions to train a deformable shape model to aid in automated hearing aid componentry placement (approximately 26% on the first mode and 51% in the first three modes). That is, doubling the dataset size had little effect on the relative importance of the first few modes. This suggests that these modes are a good indication of variation in the population as a whole. Beyond the first nine modes, the variation explained by each mode is less than what you would expect from random data, and the usefulness of these modes to describe real statistical shape variation is questionable.

By varying the weights of the eigenvectors, new shape instances created from the model are well defined and similar to those used in the training set. Furthermore,

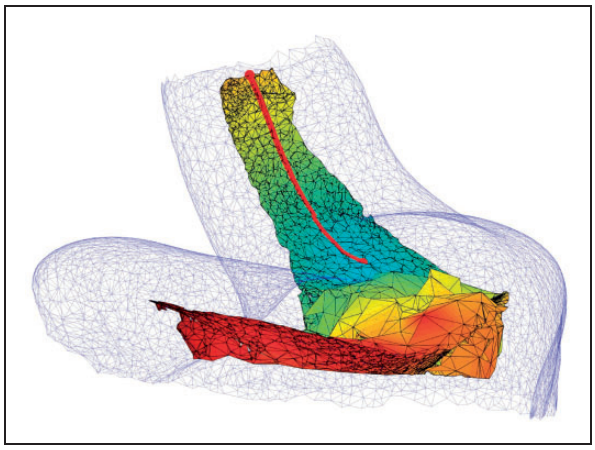

Figure 3. Plot of shortest path between two points on the mean left ear medial sheet using the fast marching algorithm.

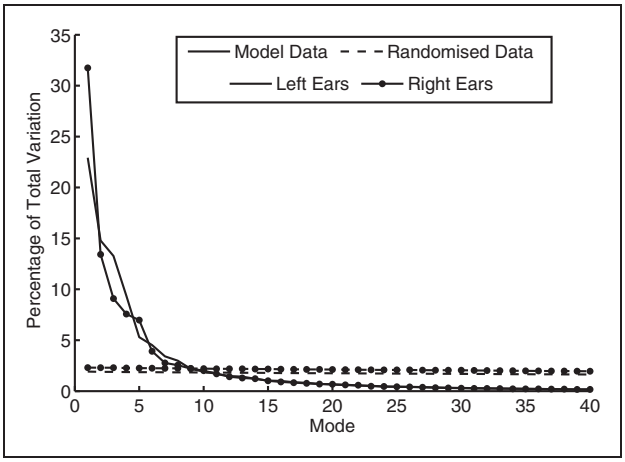

Figure 4. Plot of the percentage of total variation explained by each mode of variation in the left ear and right ear training dataset, as well as results expected from randomizing the dataset.

data within the training set can be reproduced by the model accurately using a limited number of modes. Pairwise plots of the first five eigenvector weights b used to recreate the shape instances in the training dataset indicate that we can treat these modes as independent of one another. No statistically significant correlation existed between any of the first 48 most important modes of the ear shape models. That is, the probability p of getting a correlation between any two modes as large as the observed value by random chance, when the true correlation is zero is greater than 0.05.

Cross-sectional Area

The cross-sectional area against distance from first ear canal bend for the ±3 standard deviations on the first three modes is shown in Figure 5. Highlighted is the cross-sectional area profile of the mean left and right ear (solid gray and black lines, respectively) and the narrowest left and right ear shape instances (dashed gray and black lines, respectively). Both of these instances occurred on the ±3 standard deviations of mode 1, and the widest ear canals were also observed on this mode. The mean distance along the centerline to the second bend is shown. The modal effects on the distance between first and second bend and the cross-sectional area at each mode are shown in Table 1.

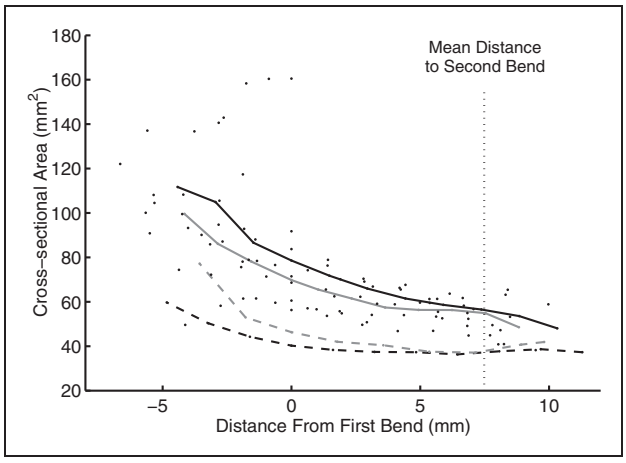

Figure 5. Scatter plot of the cross-sectional area against distance from first ear canal bend along ear canal centerline. Solid gray and black lines are the cross-sectional profile of the mean left and right ear shapes, respectively. Dashed gray and black lines are the cross-sectional profile of the narrowest left and right ear studied.

There is a narrowing down the ear canal toward the second bend on all the shapes studied (Figure 5). The area of the ear canal toward the end ranged from 36.4 to 65.4 mm^2. Both mean left and right ears were narrowest at the end, with an area of approximately 48 mm^2.

Estimated Available Vents

The cross section of the receiver element is also likely to reduce the usable cross-sectional area at the ear canal's narrowest point. For this reason, the available cross-sectional area was reduced by 7.29 mm^2, corresponding to a receiver with dimension matching that of an Oticon Digifocus II CIC hearing aid ($2.7 \times 2.7 \times 5.9$ mm; Smørum, Denmark). Knowing the minimum cross-sectional area available for vents, we can approximate how many small circular vents would fit by estimating the relative packing density of the circles.

It has been shown that the most efficient packing of circles in a plane is in a hexagonal lattice, achieving a packing density of approximately 0.906 (Chang & Wang, 2010; Thue, 1910; Tóth, 1943). Optimal packing within bounded areas is seen to be less area efficient depending on the bounding area and the size of the circles. Exact mathematical solutions exist to the circle packing problem for small numbers of circles bounded by circles and squares (Fodor, 2000, 2003; Graham, 1968; Melissen, 1994; Nurmela & Östergård, 1999; Peikert, Würtz,

Table 1. Cross-sectional Areas and Distance Between the First and Second Bends of the ±3 Standard Deviation Outputs on the First Three Modes of the Left and Right Ear Shape Models.

			Mode 1		Mode 2		Mode 3	
Measure	Ears	*M*	+3 *SD*	−3 *SD*	+3 *SD*	−3 *SD*	+3 *SD*	−3 *SD*
Distance between first and second bend (mm)	Left	7.5	5.4	8.9	8.4	6.9	6.3	6.7
	Right	8.8	9.7	6.1	7.1	8.3	7.1	6.9
Cross-sectional area at first bend (mm^2)	Left	69.8	–	46.3	83.7	56.3	60.6	71.5
	Right	78.6	40.3	–	75.4	68.6	91.8	56.7
Cross-sectional area at second bend (mm^2)	Left	54.9	59.5	40.7	65.4	44.8	53.7	58.3
	Right	53.6	38.7	63.7	44.9	63.2	56.7	52.3

Note. Dashes represent where a valid cross section could not be obtained.

Monagan, & Groot, 1992; Pirl, 1969). A referenced summary of the best-known solutions (although not always proven optimal) for packing of N equal-sized circles in circles and squares, up to $N = 1{,}500$ and $N = 10{,}000$, respectively, can be found on Specht's Web site www.packomania.com. Solutions for a variety of other geometrical domains are also available in the literature (Birgin, Bustamante, Callisaya, & Martínez, 2013; Birgin & Gentil, 2010; Galiev & Lisafina, 2013; Specht, 2013). For a review of literature on circle packing problems, see Hifi and M'Hallah (2009). Of particular interest to this research, given the approximate shape of a human ear canal, is Birgin et al.'s (2013) work on packing circles into ellipses. Birgin et al. found lower bound packing density of ellipses ranged from 0.44 to 0.83 with varying ellipse dimensions. Although the ear canal is not perfectly elliptical and the hearing aid receiver provides a packing obstacle, a conservative packing density of approximately 0.4 seems reasonable.

To test this assumption, a hexagonal lattice pattern fill of 0.4-mm vents (outside diameter 0.8 mm) was applied to a narrowest ear canal cross section of 36.4 mm^2 (Figure 6). A total of 30 vents were found to fit using the pattern given a packing density of approximately 0.5. Packing densities of larger vents were seen to be lower with 2- and 3-mm vents only achieving packing densities of approximately 0.46 and 0.31, respectively, on the same cross section.

The estimated number of vents N of varying diameters that could fit into the narrowest ear assuming a given packing density from 0.3 to 0.7 is shown in Table 2. Calculations assume that vents are spaced by at least 0.4 mm. Also shown for comparison is an equivalent vent diameter d_{eq} for a traditional single vent with equivalent area. We see that even if we assume a conservative packing density of 0.4, the estimated total vent area available will match that of a traditional 2-mm vent.

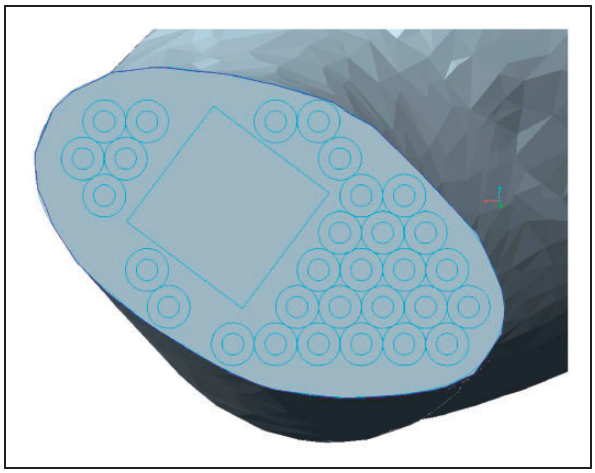

Figure 6. Sketched hexagonal packed 0.4-mm vents on narrowest ear canal cross section, square representing the hearing aid receiver element.

Spatial Design Flexibility

To determine the spatial design flexibility provided by a multivented hearing aid, 3D computer-aided design models of two in-the-canal or minicanal hearing aid models have been created. The hearing aid shell shape used for both models was based on the mean right ear mesh determined by the statistical shape model. Models also include electronic components in gray representing an A10 hearing aid battery as well as the chipset and receiver of an Oticon Digifocus II CIC hearing aid. Model A is a multivented hearing aid incorporating 16, 0.5-mm hearing aid vent paths ranging from 11.8 to 19.3 mm long (Figure 7). Model B is a single-vented hearing aid with a large 3-mm vent, 16.2 mm in length (Figure 8).

Figures 9 and 10 show views of the models A and B with the end and base plates removed. There is potentially more space for venting within the multivented model. However, 16 vents (equivalent to a 2-mm single vent) were chosen, and there is a clear view of the vent layout. The large vent used in model B causes the other componentry of the hearing aid to be located more toward the right of the model (Figures 7 to 10). The size of the vent was largely set by how compact the other componentry elements could be positioned, as a single large area is required. In contrast, we see that the multiple vented earmold has the smaller vents located in the gaps around the outside of the model. The multiple vents fit in around the important electronic componentry more easily and are able to fill the free space in the shell the larger vents are not. This provides considerable flexibility of location, shape, and size of the other hearing aid commentary within the hearing aid shell. This is particularly important as new technologies such as inductive power charging are beginning to be implemented in hearing aid products.

Manufacturability and Maintenance

Figures 9 and 10 show the multiple vents as tubes separate from the hearing aid outer shell. This could be achieved through a series of tube vent paths (i.e., made of tubing) placed within the hearing aid shell. Other options include forming the vent paths within the hearing aid shell using 3D printing technique. This is not likely to be a major barrier because currently many of the hearing aid manufacturers are moving toward 3D printing. The maintenance of a multivented device presents a challenge in terms of keeping vent paths clear. Small vent paths are likely to become blocked more

Table 2. Estimated Number of Possible Vents *N* of Varying Vent Diameters Assuming a Given Circle Packing Density.

	Packing density									
	0.3		0.4		0.5		0.6		0.7	
Vent diameter	*N*	d_{eq}	*N*	d_{eq}	*N*	d_{eq}	*N*	d_{eq}	*N*	d_{eq}
3 mm	0	0	1	3.0	1	3.0	1	3.0	2	4.2
2 mm	1	2.0	2	2.8	3	3.5	3	3.5	4	4.0
1 mm	5	2.2	7	2.6	9	3.0	11	3.3	13	3.6
0.8 mm	7	2.1	10	2.5	12	2.8	15	3.1	18	3.4
0.6 mm	11	2.0	14	2.2	18	2.5	22	2.8	25	3.0
0.5 mm	13	1.8	18	2.1	22	2.3	27	2.6	32	2.8
0.4 mm	17	1.6	23	1.9	28	2.1	34	2.3	40	2.5

Note. Area equivalent single vent diameter (d_{eq}, in mm) is also shown.

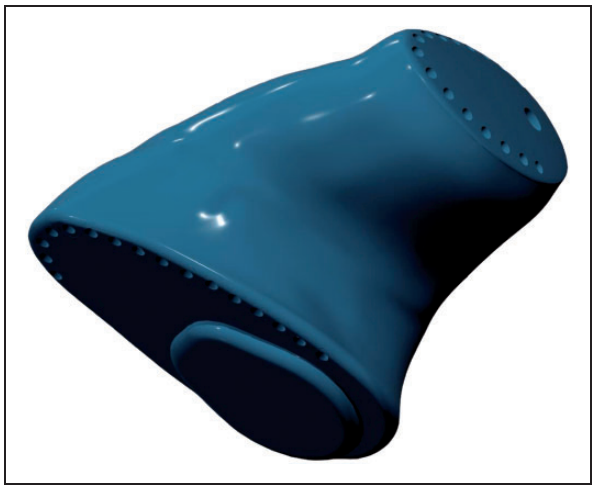

Figure 7. 3D model A of right ear ITC hearing aid incorporating 16, 0.5-mm vents.

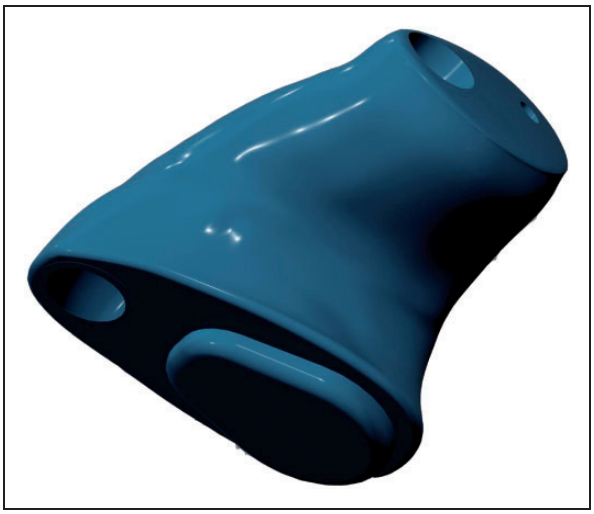

Figure 8. 3D model B of right ear ITC hearing aid incorporating a single, large 3-mm vent.

easily by wax buildup in the ear. Product design may have to include some form of wax filter or wax guard and simple vent path cleaning tools provided.

Conclusions

Investigations into the cross-sectional profile of the narrowest sections of the human ear canal shapes identified by the statistical shape model have shown that multiple venting is spatially feasible within the expected variances of the human ear. It is expected that the maximum total vent area available to a multiple vented hearing aid is at least as much as a traditional 2-mm vent. This has been validated in 3D space using 3D solid modeling of a multiple vented right ear hearing aid.

Comparative 3D model representations of two identical hearing aid shells fitted with a single large 3-mm and 16, 0.5-mm multiple vents have demonstrated the potential spatial design flexibility provided by a multiple vented hearing aid. Venting within the multiple vented hearing aid was able to easily fit around other electronic components within the hearing aid shell. This increased the design flexibility around the shape and placement of the other elements within the hearing aid shell. It may also be used alongside other technologies to improve flexibility of design in hearing aids such as inductive power charging without providing physical limitations on their implementation. Traditional hearing aid shell manufacture combined with multiple tube vents or 3D printing have been identified as possible manufacturing methods for creating multiple vented hearing aid shells. The major challenge faced by a multiple vented hearing aid has been identified as avoiding vent blockages. As such, wax blockage prevention measures such as wax guards as well as appropriate vent cleaning tools have been recommended.

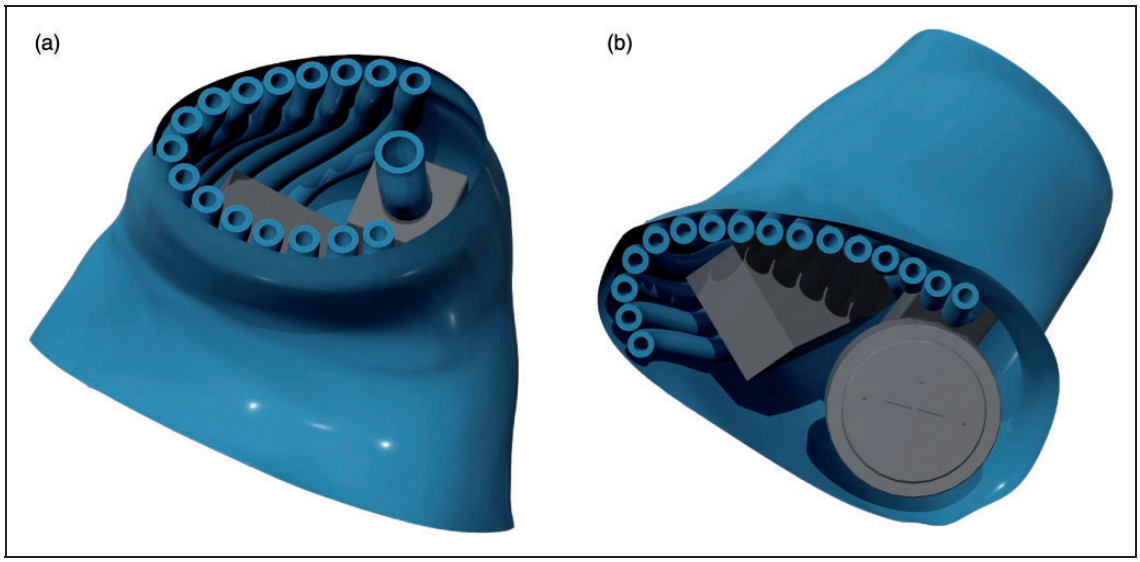

Figure 9. Views of the (a) top and (b) bottom of the hearing aid model A with the base and end plates removed.

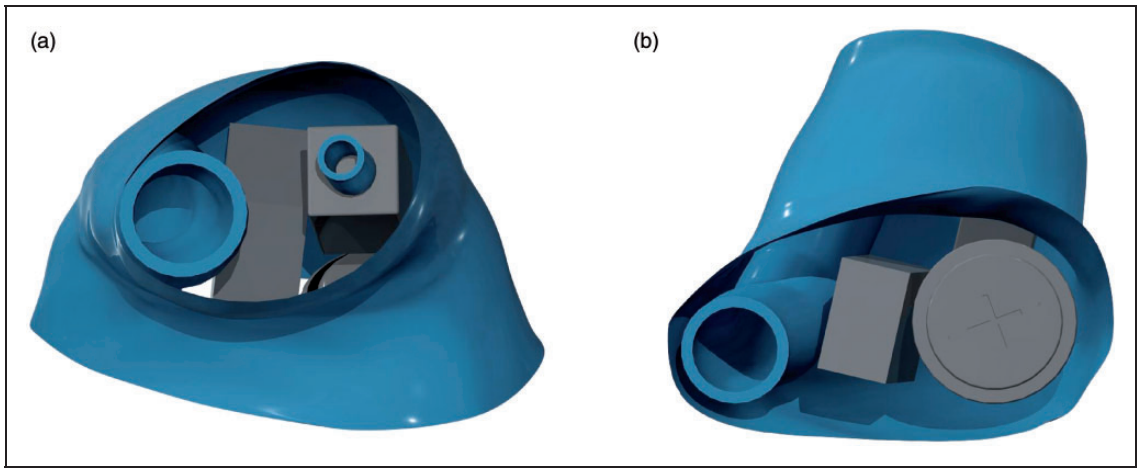

Figure 10. Views of the (a) top and (b) bottom of the hearing aid model B with the base and end plates removed.

Declaration of Conflicting Interests

The authors declared no potential conflicts of interest with respect to the research, authorship, and/or publication of this article.

Funding

Funding has been provided by the University of Auckland Doctoral Scholarship and the NZ Materials Accelerator funded by the New Zealand Foundation of Research, Science and Technology.

References

Antiga, L., Ene-Iordache, B., & Remuzzi, A. (2003, February). *Centerline computation and geometric analysis of branching tubular surfaces with application to blood vessel modeling*. Paper presented at the Meeting of WSCG POSTERS Proceedings, Campus Bory, Plzen-Bory, Czech Republic.

Beristain, A., Graña, M., & Gonzalez, A. I. (2012). A pruning algorithm for stable Voronoi skeletons. *Journal of Mathematical Imaging and Vision*, *42*(2–3), 225–237. doi: 10.1007/s10851-011-0291-1.

Birgin, E. G., Bustamante, L. H., Callisaya, H. F., & Martínez, J. M. (2013). Packing circles within ellipses. *International Transactions in Operational Research*, *20*(3), 365–389. doi: 10.1111/itor.12006.

Birgin, E. G., & Gentil, J. M. (2010). New and improved results for packing identical unitary radius circles within triangles, rectangles and strips. *Computers and Operations Research*, *37*(7), 1318–1327. doi: 10.1016/j.cor.2009.09.017.

Bookstein, F. E. (1989). Principal warps: Thin-plate splines and the decomposition of deformations. *IEEE Transactions on Pattern Analysis and Machine Intelligence*, *11*(6), 567–585.

Cárdenes, R., Bogunovic, H., & Frangi, A. F. (2010, September). *Fast 3D centerline computation for tubular structures by front collapsing and fast marching*. Paper presented at the 17th IEEE International Conference on Image Processing, ICIP 2010, Hong Kong, China.

Chang, H., & Wang, L. (2010). A simple proof of Thue's theorem on circle packing. *ArXiv e-prints, arXiv*, 1009.4322v1. Retrieved from http://arxiv.org/abs/1009.4322.

Chaussard, J., Couprie, M., & Talbot, H. (2009, September/October). *A discrete λ-medial axis*. Paper presented at the Meeting of 15th IAPR International Conference on Discrete Geometry for Computer Imagery, DGCI, Montreal, QC.

Chaussard, J., Couprie, M., & Talbot, H. (2011). Robust skeletonization using the discrete λ-medial axis. *Pattern Recognition Letters*, *32*(9), 1384–1394. doi: 10.1016/j.patrec.2010.09.002.

Chazal, F., & Lieutier, A. (2005). The "λ-medial axis". *Graphical Models*, *67*(4), 304–331. doi: 10.1016/j.gmod.2005.01.002.

Cootes, T. F., Edwards, G. J., & Taylor, C. J. (1998, June). *Active appearance models*. Paper presented at the 5th European Conference on Computer Vision—ECCV'98, Freiburg, Germany.

Cootes, T. F., Edwards, G. J., & Taylor, C. J. (2001). Active appearance models. *IEEE Transactions on Pattern Analysis and Machine Intelligence*, *23*(6), 681–685.

Cootes, T. F., Taylor, C. J., Cooper, D. H., & Graham, J. (1995). Active shape models: Their training and application. *Computer Vision and Image Understanding*, *61*(1), 38–59.

Crimi, A., Lillholm, M., Nielsen, M., Ghosh, A., De Bruijne, M., Dam, E. B.,. . . ,Sporring, J. (2011). Maximum a posteriori estimation of linear shape variation with application to vertebra and cartilage modeling. *IEEE Transactions on Medical Imaging*, *30*(8), 1514–1526.

Dey, T. K., & Zhao, W. (2003). Approximating the medial axis from the Voronoi diagram with a convergence guarantee. *Algorithmica (New York)*, *38*(1), 179–200. doi: 10.1007/s00453-003-1049-y.

Dillon, H. (2001). Hearing aid earmolds, earshells and coupling systems. In H. Dillon (Ed.), *Hearing aids* (pp. 117–158). Turramurra, NSW: Boomerang Press.

Fabbri, R., Estrozi, L. F., & Costa, L. D. F. (2002). On Voronoi diagrams and medial axes. *Journal of Mathematical Imaging and Vision*, *17*(1), 27–40. doi: 10.1023/a:1020722624682.

Fodor, F. (2000). The densest packing of 12 congruent circles in a circle. *Beiträge zur Algebra und Geometrie*, *41*(2), 401–409.

Fodor, F. (2003). The densest packing of 13 congruent circles in a circle. *Beiträge zur Algebra und Geometrie [Contributions to Algebra and Geometry]*, *44*(2), 431–440.

Galiev, S. I., & Lisafina, M. S. (2013). Linear models for the approximate solution of the problem of packing equal circles into a given domain. *European Journal of Operational Research*, *230*(3), 505–514. doi: 10.1016/j.ejor.2013.04.050.

Gerig, G., Styner, M., Shenton, M. E., & Lieberman, J. A. (2001, October). *Shape versus size: Improved understanding of the morphology of brain structures*. Paper presented at the Proceedings of MMBIA 2001, IEEE Computer Society, Utrecht, The Netherlands.

Graham, R. L. (1968). Sets of points with given maximum separation (Problem E1921). *American Mathematical Monthly*, *75*(2), 192–193.

Hifi, M., & M'Hallah, R. (2009). A literature review on circle and sphere packing problems: Models and methodologies. *Advances in Operations Research*, Article ID 150624, 22 pages, doi: 10.1155/2009/150624.

Hutton, T. J., Buxton, B. F., & Hammond, P. (2001, December). *Dense surface point distribution models of the human face*. Paper presented at the Workshop on Mathematical Methods in Biomedical Image Analysis, Kauai, HI.

Jolliffe, I. T. (1986). *Principal component analysis* (2nd ed.). NY: Springer-Verlag.

Kiessling, J., Brenner, B., Jespersen, C. T., Groth, J., & Jensen, O. D. (2005). Occlusion effect of earmolds with different venting systems. *Journal of the American Academy of Audiology*, *16*(4), 237–249. doi: 10.3766/jaaa.16.4.5.

Kuk, F., Keenan, D., & Lau, C. C. (2005). Vent configurations on subjective and objective occlusion effect. *Journal of the American Academy of Audiology*, *16*(9), 747–762.

Kuk, F., Keenan, D., & Lau, C. C. (2009). Comparison of vent effects between a solid earmold and a hollow earmold. *Journal of the American Academy of Audiology*, *20*(8), 480–491.

Kuk et al., 2005 Kuk, F., Keenan, D., Lau, C. C., Dinulescu, N., Cortez, R., & Keogh, P. (2005). Real-world performance of a reverse-horn vent. *Journal of the American Academy of Audiology*, *16*(9), 653–661.

Lorenz, C., & Krahnstöver, N. (2000). Generation of point-based 3D statistical shape models for anatomical objects. *Computer Vision and Image Understanding*, *77*(2), 175–191.

Melissen, H. (1994). Densest packings of eleven congruent circles in a circle. *Geometriae Dedicata*, *50*(1), 15–25. doi: 10.1007/bf01263647.

Miklos, B., Giesen, J., & Pauly, M. (2010, July). *Discrete scale axis representations for 3D geometry*. Paper presented at the ACM Transactions on Graphics Proceedings of ACM SIGGRAPH 2010, LA.

Nurmela, K. J., & Östergård, P. R. J. (1999). More optimal packings of equal circles in a square. *Discrete and Computational Geometry*, *22*(3), 439–457.

Ogniewicz, R., & Ilg, M. (1992, June). *Voronoi skeletons: Theory and applications*. Paper presented at the Proceedings of the IEEE Conference on Computer Vision and Pattern Recognition, Champaign, IL.

Paulsen, R., Larsen, R., Nielsen, C., Laugesen, S., & Ersbøll, B. (2002, September). *Building and testing a statistical shape model of the human ear canal*. Paper presented at the Medical Image Computing and Computer-Assisted Intervention—MICCAI 2002, Tokyo, Japan.

Peikert, R., Würtz, D., Monagan, M., & Groot, C. (1992). Packing circles in a square: A review and new results. In L. D. Davisson, A. G. J. MacFarlane, H. Kwakernaak,

J. L. Massey, Y. Tsypkin, A. J. Viterbi, & P. Kall (Eds.),, *System modelling and optimization* (vol. 180, pp. 45–54). Berlin, Germany: Springer Berlin Heidelberg.

Pirl, U. (1969). Der Mindestabstand von n in der Einheitskreisscheibe gelegenen Punkten. *Mathematische Nachrichten*, *40*, 111–124.

Pizer, S. M., Thall, A. L., & Chen, D. T. (1999). *M-reps: A new object representation for graphics* (Technical Report TR99-030). Chapel Hill: University of North Carolina.

Rouchdy, Y., & Cohen, L. D. (2011, March 30–April 2). *A geodesic voting method for the segmentation of tubular tree and centerlines*. Paper presented at the 8th IEEE International Symposium on Biomedical Imaging: From Nano to Macro, Chicago, IL.

Specht, E. (2013). High density packings of equal circles in rectangles with variable aspect ratio. *Computers and Operations Research*, *40*(1), 58–69. doi: 10.1016/j.cor.2012.05.011.

Stevenson, D., Searchfield, G., Dodd, G., & Xu, X. (2013). An experimental study on multiple acoustic venting for hearing aid applications. *Acta Acustica united with Acustica*, *99*(4), 598–606. 10.3813/aaa.918639.

Stuart, A., Allen, R., Downs, C. R., & Carpenter, M. (1999). The effects of venting on in-the-ear, in-the-canal, and completely-in-the-canal hearing aid shell frequency responses: Real-ear measures. *Journal of Speech, Language, and Hearing Research*, *42*(4), 804–813.

Studebaker, G. A., & Cox, R. M. (1977). Side branch and parallel vent effects in real ears and in acoustical and electrical models. *Journal of the American Auditory Society*, *3*(2), 108–117.

Styner, M., & Gerig, G. (2001a, June). *Medial models incorporating object variability for 3D shape analysis*. Paper presented at the Information Processing in Medical Imaging 17th International Conference, IPMI 2001, Davis, CA.

Styner, M., & Gerig, G. (2001b, December). *Three-dimensional medial shape representation incorporating object variability*. Paper presented at the 2001 IEEE Computer Society Conference, Kauai, HI.

Tam, R., & Heidrich, W. (2003, October). *Shape simplification based on the medial axis transform*. Paper presented at the VIS 2003 Proceedings, Seattle, WA.

Thue, A. (1910). Über die dichteste Zusammenstellung von kongruenten Kreisen in einer Ebene [On the densest packing of congruent circles in the plane]. *Christiana Videnskabs-Selskabs Skrifter*, *1*, 3–9.

Tóth, L. F. (1943). Über die dichteste Kugellagerung. *Mathematische Zeitschrift*, *48*, 676–684.

Valente, M., Hosford-Dunn, H., & Roeser, R. J. (2008). *Audiology treatment* (2nd ed.). New York, NY: Thieme Medical.